PHYSICAL REVIEW A **80**, 011807(R) (2009)

Wavelength dependence of high-order harmonic generation with independently controlled ionization and ponderomotive energy

Kenichi L. Ishikawa,[1,2,*] Eiji J. Takahashi,[3] and Katsumi Midorikawa[3]

[1]*Integrated Simulation of Living Matter Group, RIKEN Computational Science Research Program, 2-1 Hirosawa, Wako, Saitama 351-0198, Japan*

[2]*Precursory Research for Embryonic Science and Technology (PRESTO), Japan Science and Technology Agency, Honcho 4-1-8, Kawaguchi-shi, Saitama 332-0012, Japan*

[3]*Extreme Photonics Research Group, RIKEN Advanced Science Institute, 2-1 Hirosawa, Wako, Saitama 351-0198, Japan*

(Received 19 November 2008; published 22 July 2009)

We theoretically study the scaling with the driving wavelength λ of the high-order harmonic generation (HHG) under the simultaneous irradiation of an extreme ultraviolet (xuv) pulse. Surprisingly, when the cut-off energy and ionization yield are fixed, the harmonic yield is nearly independent of λ. We identify its origin as the combination of the initial spatial width of the states excited by the xuv pulse, making the wave packet spreading less prominent and the shallowing of the ionization potential, which suggests complex nature of the wavelength dependence of HHG.

DOI: 10.1103/PhysRevA.80.011807 PACS number(s): 42.65.Ky, 42.50.Hz, 32.80.Rm, 32.80.Fb

High-order harmonic generation (HHG) represents one of the best methods to produce ultrashort coherent light covering a wavelength range from the vacuum ultraviolet to the soft x-ray region. HHG has successfully opened new research areas, such as attosecond science [1,2] and nonlinear optics in the extreme ultraviolet (xuv) region [3,4]. The maximal harmonic photon energy E_c is given by the cut-off law $E_c=I_p+3.17U_p$ [5,6], where I_p is the ionization potential of the target atom, and $U_p[\mathrm{eV}]=F^2/4\omega^2=9.337\times10^{-14}I\ [\mathrm{W/cm^2}](\lambda\ [\mu\mathrm{m}])^2$ the ponderomotive energy, with F, I, and λ being the strength, intensity, and wavelength of the driving field, respectively. Since U_p scales as λ^2, the laser wavelength is an effective control knob for the ponderomotive energy and the cutoff, and a promising route to generate harmonics of higher photon energy is to use a driving laser of a longer wavelength. This has motivated HHG experiments with high-power midinfrared lasers [7–9]. Using a 1.55 μm driving laser field from an optical parametric amplifier [8], for example, Takahashi *et al.* [10] recently succeeded in generating harmonics with a photon energy of 300 eV from Ne and 450 eV from He gas, which lie well in the water-window region.

Under such a circumstance, the dependence of the HHG yield on λ has become an issue of increasing interest. Although it had been commonly assumed that the HHG efficiency scaled as λ^{-3} due to the spreading of the returning wave packet [11], recent theoretical [12–16], as well as experimental [7,8] studies have revealed much stronger dependence of $\propto\lambda^{-x}$ with $5\leq x\leq 6$. It is considered that the additional factor λ^{-2} is of an apparent nature stemming from the distribution of the HHG energy up to the cutoff ($\propto\lambda^2$) [13,14] although the precise physical origin of the scaling law has not been fully understood yet.

While most of the experiments are conducted with a driving laser of a single wavelength, the control of HHG using xuv pulses has also been discussed [17–21]. For example, Schafer *et al.* [17] showed that the delay of attosecond pulse trains can be used to microscopically select a single quantum path contribution. On the other hand, Ishikawa [18,19] theoretically showed that the irradiation of the xuv pulse with a photon energy $\hbar\omega_x$ smaller than I_p can boost the ionization Y_I and harmonic yield Y_H by orders of magnitude; the xuv pulse facilitates optical-field ionization by promoting a transition to (real or virtual) excited states. This effect has been experimentally demonstrated by the use of mixed gases [20]. One of the remarkable features of this effect is that Y_I increases in proportion to the xuv intensity *without affecting the cut-off energy determined by the driving infrared pulse* (Fig. 1). Thus, the addition of xuv pulses can be viewed as a tool to enable independent control of λ, E_c, and Y_I; for a

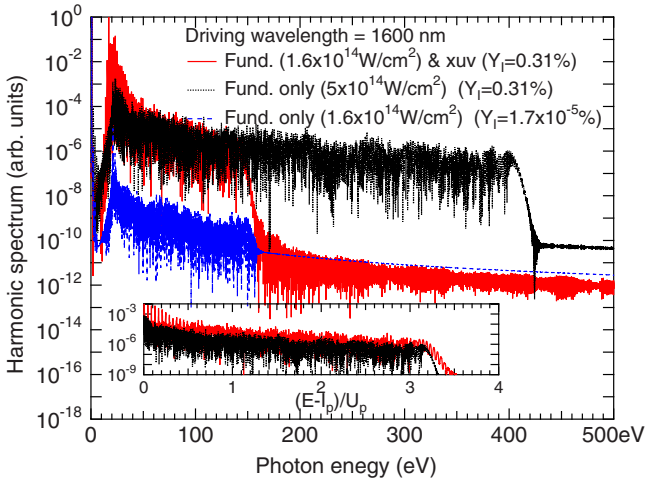

FIG. 1. (Color online) Upper solid curve: harmonic spectrum from He exposed to a 35 fs Gaussian combined driving and xuv pulse ($\hbar\omega_x=17.05$ eV), the former ($\lambda=1600$ nm) with a peak intensity of 1.6×10^{14} W/cm^2 and the latter 2.3×10^{11} W/cm^2. Middle dotted and lower dashed curves: harmonic spectra for the cases of the driving pulse alone, with an intensity of 5×10^{14} W/cm^2 and 1.6×10^{14} W/cm^2, respectively. Inset: replots of the upper two curves in terms of $(\hbar\omega_h-I_p)/U_p$.

*ishiken@riken.jp

given value of λ, E_c can be adjusted through I and then Y_I through the xuv intensity. This would provide the investigation of the λ dependence of the HHG with additional degrees of freedom.

The above consideration has motivated us to theoretically investigate the driving-wavelength dependence of HHG with the xuv control of $E_c(U_p)$ and Y_I. For the case of the driving laser pulse alone, if we fix E_c at each driving wavelength, the driving intensity is lowered with an increasing wavelength, leading to the drop of Y_I, which in turn largely affects the HHG efficiency. The addition of an xuv pulse of appropriate intensity, however, can adjust Y to a constant value, and then, we would expect $\propto\lambda^{-3}$ scaling due to the wave-packet spreading. Our results based on numerical solution of the time-dependent Schrödinger equation (TDSE), however, show that the harmonic yield is nearly independent of λ at fixed ponderomotive energy and ionization. Using the Lewenstein model [11], we identify the origin of this surprising feature as the combination of the initial spatial width of the wave function and shallowing of the effective ionization potential, indicating complex nature of the λ dependence of HHG.

To study the single-atom response under a combined driving laser and xuv pulse, we solve the TDSE in the length gauge,

$$i\frac{\partial\psi(\mathbf{r},t)}{\partial t} = \left\{-\frac{1}{2}\nabla^2 + V(r) + z[E(t) + E_x(t)]\right\}\psi(\mathbf{r},t), \quad (1)$$

for a model atom in the single active electron approximation, represented by an effective potential [22],

$$V(r) = -[1 + \alpha e^{-r} + (Z - 1 - \alpha)e^{-\beta r}]/r, \quad (2)$$

where Z denotes the atomic number. For He, we use parameters $Z=2$, $\alpha=0$, and $\beta=2.157$, which faithfully reproduce the eigenenergies of the ground and the first excited states. $E(t)=Ff(t)\sin\omega t$ is the driving optical field, with F being the peak amplitude and $f(t)$ as the envelope function corresponding the Gaussian profile with a full width at half maximum (FWHM) of 35 fs. $E_x(t)=F_x f(t)\sin\omega_x t$ is the xuv field, with F_x being the peak amplitude. The harmonic spectrum is calculated by Fourier transforming the dipole acceleration, and the HHG yield is defined as energy radiated from the target atom per unit time [23] integrated for a fixed range of photon energy $\hbar\omega_h$, specifically from 30 to 60 eV.

Figure 1 shows the harmonic spectra from He for $\lambda=1600$ nm with and without the xuv field ($\hbar\omega_x=17.05$ eV). For the case of the driving laser alone with a peak intensity I of 1.6×10^{14} W/cm^2 (lower dashed curve), the ionization yield Y_I is very low (1.7×10^{-5}%). We can increase Y_I in two ways. First, if we augment I to 5×10^{14} W/cm^2 (middle dotted curve), Y_I reaches 0.31%, and accordingly, the harmonic yield becomes higher, which is accompanied by the increase in the cut-off energy. Alternatively, the same ionization yield can be achieved by the addition of the xuv pulse with an appropriate intensity of 2.3×10^{11} W/cm^2. In this case (upper solid line), the cutoff remains nearly unchanged. Hence, as already mentioned, the combination of the laser and xuv pulses can be used as a tool to adjust λ, $E_c(U_p)$, and Y independently. It should also be noted that the resulting harmonics have an even higher yield than those from a driving laser of higher intensity alone (middle dotted line) between 30 and 60 eV. The ratio between the two cases in this energy range is ≈3.2, which is comparable with the ratio of U_p. In addition, as is shown in the inset, the harmonic yield is distributed in a similar manner between $\hbar\omega_h=I_p$ and E_c in spite of the large difference in driving intensity and cut-off energy. We have also performed simulations for xuv pulses composed of several harmonic components, forming a pulse train, and obtained similar results (not shown). These observations are consistent with the idea that the additional scaling $\propto\lambda^{-2}$ is an apparent effect due to the harmonic energy distribution up to the cutoff.

Encouraged by these results, let us now explore how the harmonic yield variates with the driving wavelength when $U_p(\propto I\lambda^2)$ and ionization are kept constant simultaneously by the addition of an xuv pulse. Many features of HHG can be intuitively and even quantitatively explained by the semiclassical three-step model [5,6,24,25]. According to this model, an electron is lifted to the continuum at the nuclear position with no kinetic energy (*ionization*), the subsequent motion is governed classically by an oscillating electric field (*propagation*), and a harmonic is emitted upon *recombination*. The last step is independent of λ as far as a given harmonic photon energy range is concerned. The first step is fixed. Concerning the propagation step, if we neglect I_p in the saddle-point equations [11,26] or, equivalently, if we consider a classical motion of electron in an oscillating electric field starting from the origin with a vanishing initial velocity, the phases of the field upon ionization $\phi_i=\omega t_i$ and recombination $\phi_r=\omega t_r$ (t_i and t_r are the times of ionization and recombination, respectively), characterizing quantum trajectories, are a function of $\hbar\omega_h/U_p$, hence common for any value of λ, since U_p is fixed. Thus, we might expect that the comparison under the condition of fixed ionization and U_p extracts the effect of the wave-packet spreading.

In Fig. 2 we show the dependence of the xuv-assisted harmonic yield on the driving wavelength from 800 nm to 1.6 μm for several different values of xuv photon energy $\hbar\omega_x$, including 20.964 eV resonant with the transition to the first excited state, as well as for a pulse train composed of $\hbar\omega_x=17.05, 20.15, 23.25, 26.35$, and 29.45 eV with a mixing ration of 0.50:0.34:0.07:0.04:0.05. The peak intensity I is 1.6×10^{14} W/cm^2 at $\lambda=800$ nm and varied so that U_p ($\propto I\lambda^2$) remains unchanged. The xuv intensity is adjusted to yield $Y_I=1$% irrespective of λ. We can see that, apart from fluctuations due to quantum-path interference [13–16,27], the harmonic yield is nearly independent of driving wavelength, in great contrast to the common anticipation that the wave-packet spreading has a contribution $\propto\lambda^{-3}$. In this figure is also shown the result for the driving intensity fixed at 1.6×10^{14} W/cm^2; the ionization yield is adjusted again to 1% through the xuv intensity although it scarcely depends on λ. In this case, reflecting the apparent harmonic energy distribution effect, the HHG yield scales as λ^{-2}, which is much gentler than the usual λ^{-5} dependence for the case of the driving pulse alone.

In order to clarify the origin of this surprising feature, let us re-examine the wave-packet spreading during the propa-

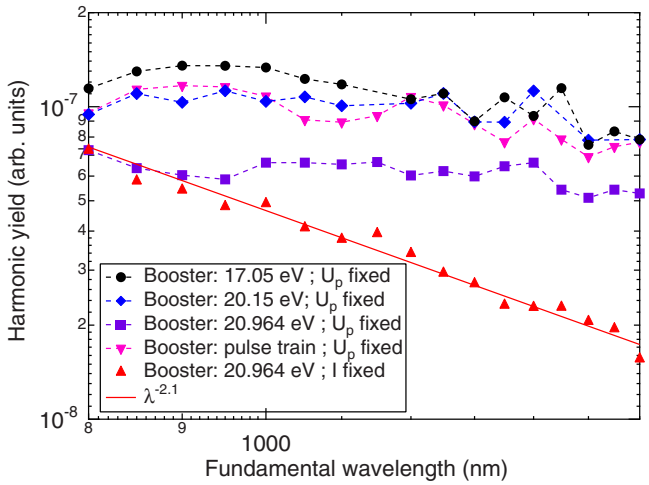

FIG. 2. (Color online) Wavelength dependence of the TDSE-calculated xuv-assisted harmonic yield from He between 30 and 60 eV for different values of $\hbar\omega_x$ as well as for a pulse train with several components (see text). $I=1.6\times10^{14}\times[(800\ \text{nm})/\lambda]^2$ W/cm^2 so that U_p may remain unchanged, except for the triangles and the fitting line, for which I is fixed at 1.6×10^{14} W/cm^2. The xuv intensity is adjusted in such a way that the ionization yield is 1% irrespective of λ.

gation process. The enhancement mechanisms under simultaneous irradiation of the xuv pulse are harmonic generation from a coherent superposition of states and two-color frequency mixing (tunneling ionization from a virtual excited state) [18,19]. The excited states are spatially much more extended than the ground state. Our discussion so far as well as the common discussion on the wavelength dependence, however, neglects the initial spatial width of the wave function. The latter can be explicitly accounted for in the Lewenstein model [11] if we approximate the ground state by a Gaussian wave function $\psi(\mathbf{r})=(\pi\Delta^2)^{-3/4}e^{-\mathbf{r}^2/(2\Delta^2)}$, where Δ $(\sim I_p^{-1})$ is the spatial width. An appealing point of this Gaussian model is that one can analytically evaluate the integral with respect to momentum in the formula for the dipole moment [Eq. (8) of Ref. [11]]. The spreading factor $(2\Delta^2+i\tau)^{-3/2}$ in the resulting formula [Eq. (22) of Ref. [11]] includes the effect of the width of the initial state.

Let us here extend the above discussion to the HHG from the superposition of the ground and an excited states, relevant to the enhancement mechanism [18,19]. Then, following Ref. [28], we obtain the formula for the dipole moment $d(t)$ as

$$d(t)=i(\Delta_g\Delta_e)^{-7/2}\int_{-\infty}^{t}dt'[2C(t,t')]^{3/2}E(t')\{A(t)A(t')+C(t,t')\{1-D(t,t')[A(t)+A(t')]\}+C^2(t,t')D^2(t,t')\}\times\exp\left\{-i[(I_pt-I_et')+B(t,t')]-\frac{A^2(t)\Delta_g^2+A^2(t')\Delta_e^2-C(t,t')D^2(t,t')}{2}\right\},\tag{3}$$

where I_e denotes the ionization potential of the excited level, Δ_g and Δ_e as the spatial width of the ground and excited states, respectively, $A(t)$ as the vector potential, and

$$B(t,t')=\frac{1}{2}\int_{t'}^{t}dt''A^2(t''),\tag{4}$$

$$C(t,t')=[\Delta_g^2+\Delta_e^2+i(t-t')]^{-1},\tag{5}$$

$$D(t,t')=A(t)\Delta_g^2+A(t')\Delta_e^2+i\int_{t'}^{t}dt''A(t'').\tag{6}$$

The factor $C^{3/2}(t,t')$ describes the leading contribution from the wave-packet spreading. For the first excited state of He ($I_e=3.6$ eV), for example, Δ_e^2 is several tens of a.u., hence comparable with the excursion time $\tau=t-t'$. This, making the wave-packet spreading relatively less prominent, is expected to influence the wavelength scaling.

It should be noted that if we resorted to the saddle-point analysis (SPA) [11,26] instead of the momentum integration, the ionization time t' would contain an imaginary part $\text{Im}\,t'\approx\sqrt{2I_e}/E(t')$ stemming from the tunneling process. Then the spreading factor would rather read as $[\Delta_g^2+\Delta_e^2+\sqrt{2I_e}/E(t')+i\tau]^{-3/2}$, containing an additional term that can be interpreted as the width at the tunnel exit [29]. This tunneling contribution is automatically accounted for in Eq. (3). Since $\Delta_g^2<\sqrt{2I_e}/E(t')<\sqrt{2I_p}/E(t')<\Delta_e^2$, in general, the width of the excited state has the largest contribution in the xuv-assisted HHG while the initial width is negligible for the case of the ground-state atom.

The form of Eq. (3) suggests that the dependence of the HHG yield on the initial spatial width of the wave function and the ionization potential is rather complex. While these two are correlated with each other in the real atom, here we treat them as independent parameters and list in Table I the exponent of the power-law scaling for different combinations of Δ_e and I_e, calculated with Eq. (3). I_e as a free parameter may be interpreted as the effective ionization potential defined by $I_e=I_p-\hbar\omega_x$. It should be noted that the peak intensity is fixed at 1.6×10^{14} W/cm^2 so the results are to be compared with the triangles in Fig. 2. Both larger initial spatial width and shallower effective ionization potential decrease the exponent, and their synergy leads to the surprising gentle wavelength scaling.

In summary, we have investigated the driving-wavelength dependence of HHG under the simultaneous irradiation of a

TABLE I. Exponent x of the wavelength scaling $\propto\lambda^{-x}$ for various combinations of the initial spatial width Δ_e and the effective ionization potential I_e.

Δ_e (a.u.)	I_e (eV)		
	3.6	4.4	13.6
5.8	2.2	2.2	4.3
4.5	2.4	2.7	4.5
3.2	2.7	3.4	4.9
1.1	4.0	4.2	5.4

nonionizing xuv pulse. The xuv pulse serves as a tool to provide additional degrees of freedom to the study of the λ dependence of HHG, with its ability to adjust the cutoff and ionization yield independently and control the initial spatial width of the wave function and the effective ionization potential. We have shown that the xuv-assisted harmonic yield scales with λ much more weakly than for the case of the driving laser alone; fixed U_p and Y, especially, lead to a very small λ dependence. According to our analysis based on the Gaussian model, the combination of the large spatial width of the states excited by the xuv pulse making the effect of the wave-packet spreading less prominent and the shallowing of the effective ionization potential is responsible for this unexpected feature. While both effects are described in Eq. (3), in principle, clear-cut explanation why the latter contributes to the gentle scaling is not at hand. The results of the present Rapid Communication indicate that the λ scaling of HHG is not simply governed by the wave-packet spreading ($\propto\lambda^{-3}$) and the apparent energy distribution effect ($\propto\lambda^{-2}$) but exhibits richer and more complex behavior than previously considered. There are indeed further open questions such as why higher-order returning trajectories have so important contribution [12–15]. Further study will be necessary to answer these questions.

K.L.I. acknowledges inspiring discussions with H. Suzuura, J. Burgdörfer, and K. Schiessl. K.L.I. also gratefully acknowledges financial support by the Precursory Research for Embryonic Science and Technology program of the Japan Science and Technology Agency and by the Ministry of Education, Culture, Sports, Science, and Technology of Japan under Grant No. 19686006. This work was financially supported by a grant from the Research Foundation for Opto-Science and Technology.

[1] M. Hentschel, R. Kienberger, Ch. Spielmann, G. Reider, N. Milosevic, T. Brabec, P. Corkum, U. Heinzmann, M. Drescher, and F. Krausz, Nature (London) **414**, 509 (2001).
[2] P. Tzallas, D. Charalambidis, N. Papadogiannis, K. Witte, and G. D Tsakiris, Nature (London) **426**, 267 (2003).
[3] T. Sekikawa, A. Kosuge, T. Kanai, and S. Watanabe, Nature (London) **432**, 605 (2004).
[4] Y. Nabekawa, H. Hasegawa, E. J. Takahashi, and K. Midorikawa, Phys. Rev. Lett. **94**, 043001 (2005).
[5] J. L. Krause, K. J. Schafer, and K. C. Kulander, Phys. Rev. Lett. **68**, 3535 (1992).
[6] K. C. Kulander, K. J. Schafer, and J. L. Krause, in *Superintense Laser-Atom Physics*, NATO Advanced Study Institute Series B: Physics, edited by B. Piraux, A. L'Huillier, and K. Rzazewski, (Plenum, New York, 1993), Vol. 316, p. 95.
[7] P. Colosimo, G. Doumy, C. I. Blaga, J. Wheeler, C. Hauri, F. Catoire, J. Tate, R. Chirla, A. M. March, G. G. Paulus, H. G. Muller, P. Agostini, and L. F. DiMauro, Nat. Phys. **4**, 386 (2008).
[8] E. J. Takahashi, T. Kanai, Y. Nabekawa, and K. Midorikawa, Appl. Phys. Lett. **93**, 041111 (2008).
[9] T. Popmintchev, M. Chen, O. Cohen, M. E. Grisham, J. J. Rocca, M. M. Murnane, and H. C. Kapteyn, Opt. Lett. **33**, 2128 (2008).
[10] E. J. Takahashi, T. Kanai, K. L. Ishikawa, Y. Nabekawa, and K. Midorikawa, Phys. Rev. Lett. **101**, 253901 (2008).
[11] M. Lewenstein, Ph. Balcou, M. Yu. Ivanov, A. L'Huillier, and P. B. Corkum, Phys. Rev. A **49**, 2117 (1994).
[12] J. Tate, T. Auguste, H. G. Muller, P. Salières, P. Agostini, and L. F. DiMauro, Phys. Rev. Lett. **98**, 013901 (2007).
[13] K. Schiessl, K. L. Ishikawa, E. Persson, and J. Burgdörfer, Phys. Rev. Lett. **99**, 253903 (2007).
[14] K. Schiessl, K. L. Ishikawa, E. Persson, and J. Burgdörfer, J. Mod. Opt. **55**, 2617 (2008).
[15] K. L. Ishikawa, K. Schiessl, E. Persson, and J. Burgdörfer, Phys. Rev. A **79**, 033411 (2009).
[16] M. V. Frolov, N. L. Manakov, and A. F. Starace, Phys. Rev. Lett. **100**, 173001 (2008).
[17] K. J. Schafer, M. B. Gaarde, A. Heinrich, J. Biegert, and U. Keller, Phys. Rev. Lett. **92**, 023003 (2004).
[18] K. Ishikawa, Phys. Rev. Lett. **91**, 043002 (2003).
[19] K. L. Ishikawa, Phys. Rev. A **70**, 013412 (2004).
[20] E. J. Takahashi, T. Kanai, K. L. Ishikawa, Y. Nabekawa, and K. Midorikawa, Phys. Rev. Lett. **99**, 053904 (2007).
[21] K. L. Ishikawa, E. J. Takahashi, and K. Midorikawa, Phys. Rev. A **75**, 021801(R) (2007).
[22] H. G. Muller, Phys. Rev. A **60**, 1341 (1999).
[23] J. D. Jackson, *Classical Electrodynamics* (Wiley and Sons, New York, 1998).
[24] K. J. Schafer, B. Yang, L. F. DiMauro, and K. C. Kulander, Phys. Rev. Lett. **70**, 1599 (1993).
[25] P. B. Corkum, Phys. Rev. Lett. **71**, 1994 (1993).
[26] D. B. Milošević and W. Becker, Phys. Rev. A **66**, 063417 (2002).
[27] D. B. Milošević, E. Hasović, S. Odžak, M. Busuladžić, A. Gazibegović-Busuladžić, and W. Becker, J. Mod. Opt. **55**, 2653 (2008).
[28] J. B. Watson, A. Sanpera, X. Chen, and K. Burnett, Phys. Rev. A **53**, R1962 (1996).
[29] B. Gottlieb, A. Lohr, W. Becker, and M. Kleber, Phys. Rev. A **54**, R1022 (1996).